POLITECNICO DI TORINO
Repository ISTITUZIONALE

Implementation of a Lag Elliptic-Blending model for RANS equations in OpenFOAM

Original
Implementation of a Lag Elliptic-Blending model for RANS equations in OpenFOAM / Gajetti, Eleonora; Marocco, Luca; Boccardo, Gianluca; Buffo, Antonio; Savoldi, Laura. - In: OPENFOAM JOURNAL. - ISSN 2753-8168. - 4:(2024), pp. 104-116. [10.51560/ofj.v4.133]

Availability:
This version is available at: 11583/2992960 since: 2024-10-07T12:35:03Z

Publisher:
OpenFOAM Journal

Published
DOI:10.51560/ofj.v4.133

Terms of use:

This article is made available under terms and conditions as specified in the corresponding bibliographic description in the repository

Publisher copyright

(Article begins on next page)

21 November 2024

OpenFOAM®
Journal

Volume 4 [18^{th} *OpenFOAM Workshop* – 2023], Pages 104–116
ISSN: 2753-8168

Implementation of a Lag Elliptic-Blending model for RANS equations in OpenFOAM

Eleonora Gajetti[1,*], Luca Marocco[2], Gianluca Boccardo[3], Antonio Buffo[3], and Laura Savoldi[1]

[1]MAHTEP Group, Energy Department ”Galileo Ferraris”, Politecnico di Torino

[2]Energy Department, Politecnico di Milano

[3]Department of Applied Science and Technology, Politecnico di Torino

Email address: eleonora.gajetti@polito.it

DOI: https://doi.org/10.51560/ofj.v4.133
Results with version(s): OpenFOAM® v2212
Repository: https://github.com/MAHTEP/EllipticBlending

Abstract. Turbulence modeling remains a significant challenge in Computational Fluid Dynamics. Achieving a balance between model accuracy and computational efficiency often leads to the widespread utilization of RANS (Reynolds Averaged Navier Stokes) turbulence models. The current study focuses on implementing the $k-\varepsilon$ Lag Elliptic Blending turbulence model within OpenFOAM®. This extension of the conventional $k-\varepsilon$ model introduces an elliptic equation to handle non-uniform behavior near walls and a transport equation to account for the lag between stress and strain tensors. Comparison of results from two benchmark cases with those obtained from the commercial software STAR-CCM+®, which also includes the model, reveals good agreement between the two codes. Consequently, the implementation can be considered verified.

1. Introduction

Within the several options for modelling turbulent flows, which span from single equation models to Direct Numerical Simulations, the RANS closures remain the most widely used as they allow adequate stability and accuracy of solutions while remaining low-expensive from a computational cost. Between them, the most adopted RANS closures, e.g. the $k-\omega$ Shear-Stress Transport (SST) model and Realizable $k-\varepsilon$ model, rely on two additional equations, one for the turbulent kinetic energy and one for the turbulent specific dissipation rate or the turbulent dissipation rate . Although these models have been extensively validated for many reference engineering cases, they may prove inaccurate for highly complex problems, such as turbulent flows in mini-channels [1]. One relevant issue with these models is the linear eddy viscosity assumption, resulting in overestimation of turbulence production when misalignment of stress and strain occurs in the flow.

Reynolds Stress Models (RSM) usually provide more accurate results for cases in which the flow anisotropy plays a major role [2], at the cost, however, of seven equations to be solved, instead of two. In 1993, Durbin [3] formulated an improved RSM version by adding six relaxation equations to represent the non-homogeneous near-wall behaviour. Durbin’s formulation was later futher developed by Manceau and Hanajalic in 2002 [4], and Lardeau and Manceau [5] in 2014, and the original six equations boiled down to only one elliptic differential equation for a blending factor. The latter is also less computationally expensive than a full transport equation. This turbulence model, referred to as Elliptic Blending Reynolds Stress Model (EBRSM), has been recently added in OpenFOAM® v2206 [6]. Its relevancy and accuracy, compared to standard models, was documented by Stoellinger et al. [7] in 2015. However, since this turbulence closure belongs to the Reynolds Stress family, it remains computationally more expensive than standard eddy viscosity models.

Lardeau and Billard [8] formulated in 2016 a new turbulence model derived from the EBRSM and the work of Revell et al. [9] of 2006. The latter proposed a $k-\varepsilon$ model with a further transport equation for the misalignment between stress and strain: a Lag $k-\varepsilon$ model. The novel Lag-EB $k-\varepsilon$ model of

[*] Corresponding author

Received: 30 December 2023, Accepted: 14 June 2023, Published: 24 July 2024

©2024 The Authors. This work is an open access article under the CC BY-SA 4.0 license

Lardeau and Billard [8] was further improved in the work of Tunstall et al. [10] and then implemented in the commercial software STAR-CCM+® [11]. It was found in [8,10] that it performed better for different benchmark cases than the $k-\varepsilon-v^2/k$ and $k-\omega$ SST models, remaining as precise as the EBRSM but computationally cheaper and numerically more stable. In 2019 Biswas et al. [12] implemented a Lag EB $k-\omega$ model in OpenFOAM® and validated it against several benchmark cases. Nevertheless, their code is not open-source and, to the authors' knowledge, there is no further evidence of Lag EB models in OpenFOAM®.

This $k-\varepsilon$ Lag EB model [8,10] bears resemblance to the $k-\varepsilon-\bar{v}^2/k$ turbulence model introduced by Billard and Laurence [13] in 2012, as well as to the "k-epsilon-phit-f" model proposed by Laurence et al. [14] in 2005. The key difference between the present model and the other two lies in the distinct definition of the lag parameter and the inclusion of a non-linear anisotropy tensor within the transport equation of the lag parameter, which is absent in [13] and [14]. Additionally, in the "k-epsilon-phit-f" model, an elliptic relaxation factor "f", with the dimensions of frequency, is employed instead of the non-dimensional elliptic blending factor. Billard and Laurence's model [13] is available in the commercial code STAR-CCM+®and in the open-source package Code Saturne [15]. Laurence's model [14] is implemented in OpenFOAM®.

This paper describes the implementation of the $k-\varepsilon$ Lag EB model in OpenFOAM® according to Tunstall et al. [10] and provides a code-to-code comparison for two benchmark cases with STAR-CCM+®, which has the same model implemented as described in the user guide [16]. This comparative approach is essential for users who rely on OpenFOAM® for industrial applications and need to understand its capabilities and limitations.

2. **Model formulation**

The Lag EB model entails slightly modified transport equations for $k-\varepsilon$ compared to the standard $k-\varepsilon$ model. It includes an additional transport equation for the lag parameter φ and an elliptic equation for the elliptic blending factor. In the original formulation by [8, 10], the elliptic blending factor was denoted as α. However, as the letter α is already utilized in OpenFOAM®, here the elliptic blending parameter is denoted as *ebf*.

The transport equations for the turbulent kinetic energy k and the turbulent dissipation rate ε are given in Eqn. 1 and Eqn. 2, respectively. Here, ρ is the density, $\mathbf{U}$ is the mean velocity, ν the molecular viscosity, ν_t the turbulent viscosity. Compared to the standard $k-\varepsilon$ model, the molecular viscosity is divided by a factor 2. The coefficients σ_k, σ_ε, $C_{\varepsilon1}$ and $C_{\varepsilon2}$ are listed in Tab. 1. The turbulent time scale $\tau = k/\varepsilon$ appears in Eqn. 2.

$$\frac{\partial(\rho k)}{\partial t} + \nabla\cdot(\rho k\mathbf{U}) = \nabla\cdot\left[\rho\left(\frac{\nu}{2}+\frac{\nu_t}{\sigma_k}\right)\nabla k\right] + \rho P - \rho\varepsilon \tag{1}$$

$$\frac{\partial(\rho \varepsilon)}{\partial t} + \nabla\cdot(\rho \varepsilon\mathbf{U}) = \nabla\cdot\left[\rho\left(\frac{\nu}{2}+\frac{\nu_t}{\sigma_\varepsilon}\right)\nabla \varepsilon\right] + \frac{\rho}{\tau}(C_{\varepsilon1}P - C_{\varepsilon2}\varepsilon) + \rho E \tag{2}$$

The turbulent production rate P in equations Eqn. 1 and Eqn. 2 is defined in Eqn. 3.

$$P = 2\nu_t S_{ij}S_{ij}; \quad S_{ij} = \frac{1}{2}\left(\frac{\partial U_i}{\partial x_j}+\frac{\partial U_j}{\partial x_i}\right) \tag{3}$$

where S_{ij} is the mean strain rate tensor.

The additional production term E in the ε equation is given in Eqn. 4.

$$E = C_k\nu\nu_t(1-ebf)^3\left(\frac{\partial|2S_{ij}n_j|n_k}{\partial x_k}\right)^2 \tag{4}$$

where n is the wall-normal unity vector [17] and C_k a coefficient listed in Tab. 1. The code snippets for E and n are given below.

```
volVectorField magTermE
(
     mag(2.0*S & n)*n
);
const volScalarField E
(
    CK_*pow3(scalar(1.0) - ebf_)*this->nu()*nut*sqr(fvc::div(magTermE))
);
```

Listing 1. Additional production term in Eqn. 4

```
const volVectorField n
(
    fvc::grad(ebf_)/max(
        mag(fvc::grad(ebf_)), dimensionedScalar(dimless/dimLength, SMALL)
        )
);
```

Listing 2. Wall-normal unity vector

The lag parameter φ is defined in Eqn. 5 and is further discussed in Appendix A. Its transport equation is given in Eqn. 6.

$$\varphi = -\frac{1}{C_\mu}\frac{A_{ij}S_{ij}}{\tilde{S}}\frac{\varepsilon}{k\tilde{S}} \tag{5}$$

$$\begin{aligned}\frac{\partial(\rho\varphi)}{\partial t} + \nabla\cdot(\rho\varphi\mathbf{U}) =& \nabla\cdot\left[\rho\left(\frac{\nu}{2}+\frac{\nu_t}{\sigma_\varphi}\right)\nabla\varphi\right]\\ &-\rho\left[(1-ebf^3C_w^*)\frac{\varphi}{\tau} - ebf^3\left(\widetilde{C}_1 + C_1^*\frac{P}{\tau} - C_{P1}\frac{P}{k}\varphi\right) + ebf^3C_{P2}\tilde{S}\varphi\right]\\ &+\rho\left[\frac{ebf^3}{S^2\tau}(C_4^*A_{ik}S_{kj} - C_5^*A_{ik}W_{kj})S_{ij} + ebf^3\frac{C_{p3}}{\tau}\right]\end{aligned} \tag{6}$$

where σ_φ, C_w^*, $\tilde{C}_1$, C_1^*, C_{P1}, C_{P2}, C_{P3}, C_4^* and C_5^* are coefficients defined in Tab. 1 and in Eqn. 14 and $\tilde{S} = \sqrt{2S_{ij}S_{ij}}$ is the strain rate magnitude.

In the above Eqn. 5 and Eqn. 6, A_{ij} is the anisotropy tensor defined by Eqn. 7:

$$A_{ij} = -2\frac{\nu_t}{k}\left[S_{ij} + 2\beta_2\frac{S_{ik}\widetilde{W}_{kj} - \widetilde{W}_{ik}S_{kj}}{\sqrt{(S_{kl}+\widetilde{W}_{kl})(S_{kl}+\widetilde{W}_{kl})}}\right] \tag{7}$$

where β_2 is a coefficient defined in Tab. 1 and in Eqn. 14, while $\widetilde{W}$ is the modified vorticity tensor, defined in Eqn. 8, that includes the curvature correction.

$$\widetilde{W}_{ij} = \frac{1}{2}\left(\frac{\partial U_i}{\partial x_j} - \frac{\partial U_j}{\partial x_i}\right) - \frac{1}{\tilde{S}^2}\left(S_{ik}\frac{DS_{jk}}{Dt} - S_{jk}\frac{DS_{ik}}{Dt}\right) \tag{8}$$

The material derivative of the strain rate appearing in the curvature correction of Eqn. 8 is given in Eqn. 9.

$$\frac{DS_{ij}}{Dt} = \frac{\partial S_{ij}}{\partial t} + u_k\frac{\partial S_{ij}}{\partial x_k} = \frac{\partial S_{ij}}{\partial t} + \frac{\partial(u_kS_{ij})}{\partial x_k} - S_{ij}\frac{\partial u_k}{\partial x_k} \tag{9}$$

The code snippets for A_{ij} and $\widetilde{W}_{ij}$ are given below.

```
volTensorField A
(
    -scalar(2.0)*nut/k_*(S + scalar(2.0)*beta2_*((S & WTilde) - (WTilde & S))/
    (mag(S + WTilde)))
);
```

Listing 3. Anisotropy tensor

```
const volSymmTensorField DSDiv_ = fvc::ddt(S)
                                + fvc::div(this->phi(), S) - S * fvc::div(U);

const volTensorField SDS
(
    (S & DSDiv_.T())/(2.0*magSqr(S))
);
const volTensorField WTilde
    (
        W - 2.0*skew(SDS)
    );
```

Listing 4. Curvature correction

As shown in Listing 4, the initial step to calculate $\widetilde{W_{ij}}$ involves computing an auxiliary symmetric tensor denoted as $DSDiv\_$, representing the $\frac{DS_{ij}}{Dt}$. Following this, the expression $\frac{1}{\tilde{S}^2}(S_{ik}\frac{DS_{jk}}{Dt})$ is evaluated, and twice its antisymmetric component is subtracted from the vorticity tensor W_{ij} to derive $\widetilde{W_{ij}}$.

The elliptic blending factor ebf is computed from Eqn. 10.

$$L^2\nabla^2 ebf = ebf - 1 \tag{10}$$

where C_L and C_η are coefficients defined in Tab. 1 and L is a turbulent length scale, defined in Eqn. 11.

$$L = C_L\sqrt{\frac{k^3}{\varepsilon^2} + C_\eta^2\sqrt{\frac{\nu^3}{\varepsilon}}} \tag{11}$$

Finally, the eddy viscosity can be computed from Eqn. 12.

$$\nu_t = C_\mu\,\varphi\,k\,\min\left(T_{\text{lim}}, \frac{1}{\sqrt{3}C_\mu\varphi\tilde{S}}\right) \tag{12}$$

where C_μ is a coefficient listed in Tab. 1 and the temporal scale for the limiter of the realizability constraint, T_{lim}, is defined in Eqn. 13.

$$T_{\text{lim}} = \sqrt{\frac{k^2}{\varepsilon^2} + C_t^2\frac{\nu}{\varepsilon}} \tag{13}$$

where C_t is a coefficient listed in Tab. 1.

All model coefficients come from Tunstall et al. [10] except C_k, which is 2.3 instead of 9.2, in agreement with [8], [15] (where the same coefficient is called C_{ε_3}) and [16]. They are all listed in Tab. 1, while those derived from these are computed in Eqn. 14.

Table 1. Model coefficients

$C_{\varepsilon 1}$	$C_{\varepsilon 2}$	C_k	σ_k	σ_ε	σ_φ	C_μ	C_T	C_L	$C\eta$	C_t	C_1	C_1^*	C_3	C_3^*	C_4	C_5	C_w
1.44	1.9	2.3	1	1.2	1	0.22	1	0.164	75	4	1.7	0.9	0.8	0.65	0.625	0.2	5

$$\begin{aligned}
C_w^* &= C_{\varepsilon 2} - 1 + C_w - \frac{1}{C_\mu} \\
\tilde{C_1} &= C_1 + C_{\varepsilon 2} - 2 \\
C_{P1} &= 2 - C_{\varepsilon 1} \\
C_{P2} &= \frac{C_3^*}{\sqrt{2}} \\
C_{P3} &= \frac{f_\mu}{C_\mu}\left(\frac{2}{3} - \frac{C_3}{2}\right) \\
C_4^* &= \frac{2}{C_\mu}(1 - C_4) \\
C_5^* &= \frac{2}{C_\mu}(1 - C_5) \\
\beta_2 &= 2\frac{1 - C_5}{C_1 + C_1^* + 1}
\end{aligned} \tag{14}$$

2.1. **Boundary conditions.** The $k - \varepsilon$ Lag EB model belongs to the low Reynolds family, therefore the first cell requires $y^+ \approx 1$. Wall functions were used for k, `kLowReWallFunction`, for ε, `epsilonWallFunction` with `lowReCorrection`, and for ν_t, `nutkWallFunction`. The lag parameter φ and the elliptic blending factor ebf are both zero at the walls. Moreover, ebf is set to `zeroGradient` at the inlet and outlet, while φ is set to `zeroGradient` at outlet and to the value of 2/3 at inlet, corresponding to isotropic turbulence.

3. Verification of the implemented model

The model implementation was verified by comparing the results obtained with OpenFOAM® with those of STAR-CCM+® for two benchmark cases: the backward-facing step (BFS), a 90° pipe bend. Moreover, a consistency check of the implementation is provided in Appendix B.

3.1. **Benchmark case: Backward-facing step.** The geometry considered matches that available on NASA's Turbulence Modeling Resource [18], for which experimental data are also available. The geometry, boundary conditions and mesh details are shown in Fig. 1. Steady-state 2D simulations for an incompressible isothermal Newtonian fluid have been carried out for $Re_H = 36000$ based on the step height. The same mesh, similar to that available in OpenFOAM® [19] and refined close to the walls to obtain $y^+ \approx 1$, as required by the $k - \varepsilon$ Lag EB model, has been used for the simulations in OpenFOAM® and in STAR-CCM+®. The solver `simpleFoam` has been adopted with the `linearUpwind` convective discretization scheme for the velocity. This scheme corresponds to a second order upwind discretization scheme in STAR-CCM+®. For the turbulent quantities a first order `upwind` scheme has been used. Uniform values of the quantities were imposed on the inlet section, with k evaluated by `turbulentIntensityKineticEnergyInlet` considering a turbulence intensity value $I = 1\%$, and epsilon by `turbulentMixingLengthDissipationRateInlet` with a mixing length value $\ell = 0.07(2H)$.

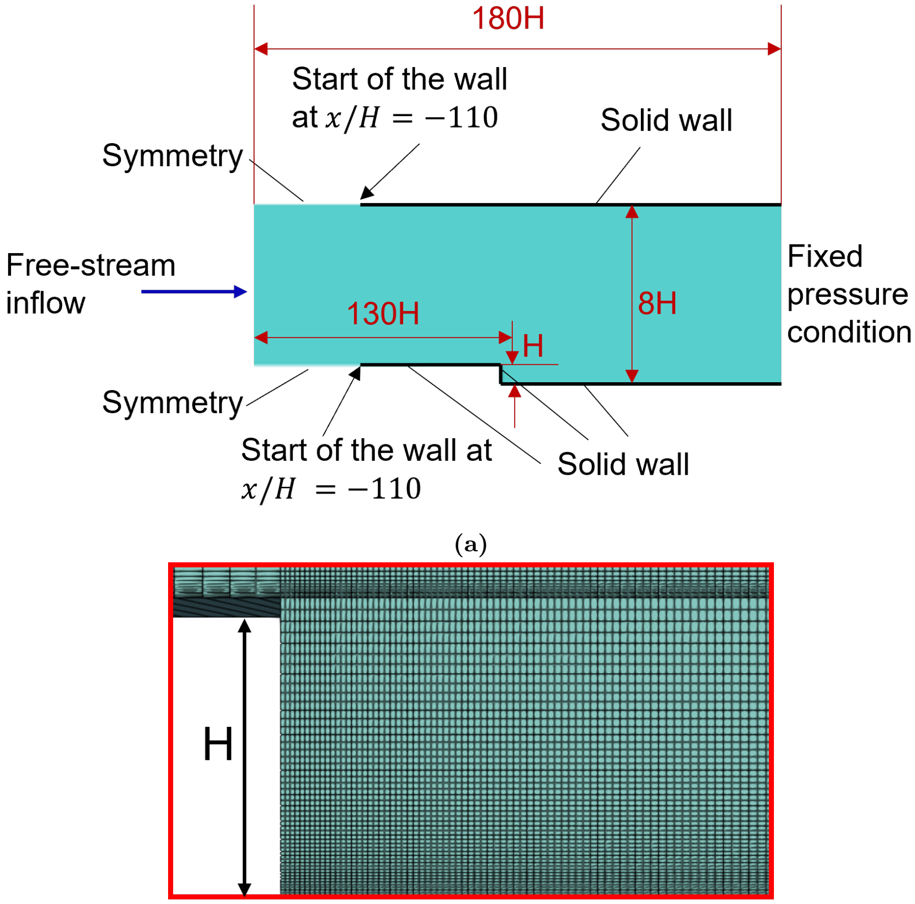

(a)

(b)

Figure 1. BFS geometry. (a) Domain extension and boundary conditions (b) Mesh details

Velocity and turbulence profiles of interest are chosen downstream of the step at $x/H = 1, 4, 6$, as highlighted in Fig. 2. A reference velocity, U_{ref}, corresponding to the center-channel value at $x/H = -4$ [19], is used to nondimensionalize velocity, pressure coefficient and turbulent quantities.

The pressure coefficient on the bottom wall, defined in Eqn. 15 and shown in Fig. 3, is practically the same for OpenFOAM® and STAR-CCM+® and also agrees well with the experimental data [18], except close to the step.

$$C_p = \frac{p}{0.5\rho U_{\text{ref}}^2} \tag{15}$$

The velocity profiles calculated with OpenFOAM® and STAR-CCM+® are practically coincident, as shown in Fig. 4. On the other hand, differences of up to 40% can be seen in the turbulent viscosity ratio, shown in Fig. 5. To investigate the cause, the profiles of the quantities contributing to the calculation of

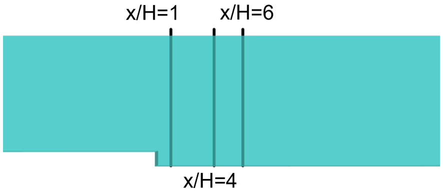

Figure 2. Sections downstream the step

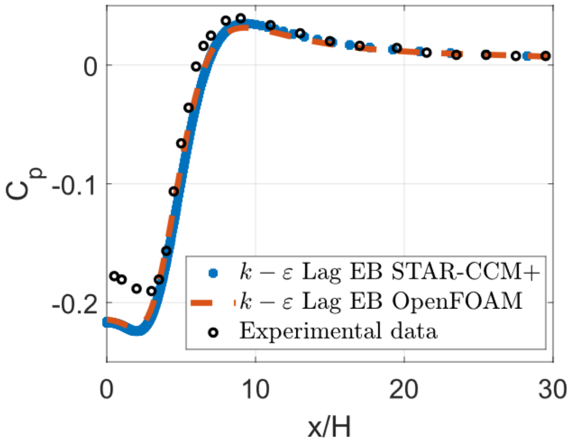

Figure 3. Pressure coefficient after the step, along the lower wall

ν_t, Eqn. 12, were also plotted, thus turbulent kinetic energy, Fig. 6, turbulent kinetic energy dissipation, Fig. 7, lag parameter, Fig. 8, and strain rate magnitude, Fig. 9. The major discrepancies between the two codes are in the values of φ, Fig. 8. Nevertheless, analysis of the results showed that the minimum between the two arguments in the calculation of ν_t, Eqn. 12, is practically always the second one. It follows that $\nu_t = \frac{k}{\sqrt{3}\tilde{S}}$, in which only k and $\tilde{S}$ appear but not ε and φ. Thus the values of k and $\tilde{S}$ calculated with OpenFOAM® and STAR-CCM+® result in the differences in ν_t. Considering that the simulations with both codes use the same convective discretization schemes and the SIMPLE algorithm for pressure-velocity coupling, the reason for these small discrepancies is not completely clear, as there is no complete access to the source code of STAR-CCM+®. However, as already described, the differences are both small and limited to a restricted area of the domain. The verification of the implementation can therefore be considered successful.

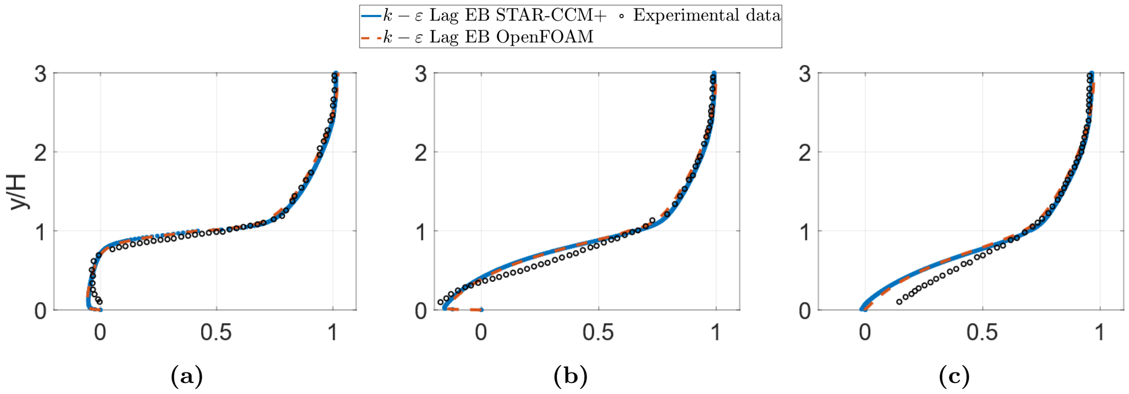

Figure 4. Normalized velocity magnitude, U/U_{ref}: (a) x/H = 1, (b) x/H = 4, (c) x/H = 6

The contours of the normalized velocity magnitude, the turbulent viscosity ratio and the lag parameter are shown in Fig. 10, Fig. 11 and Fig. 12, respectively. While the first two are qualitatively very similar, the contours of φ differ between the two codes. The reason for this discrepancy is not known to the

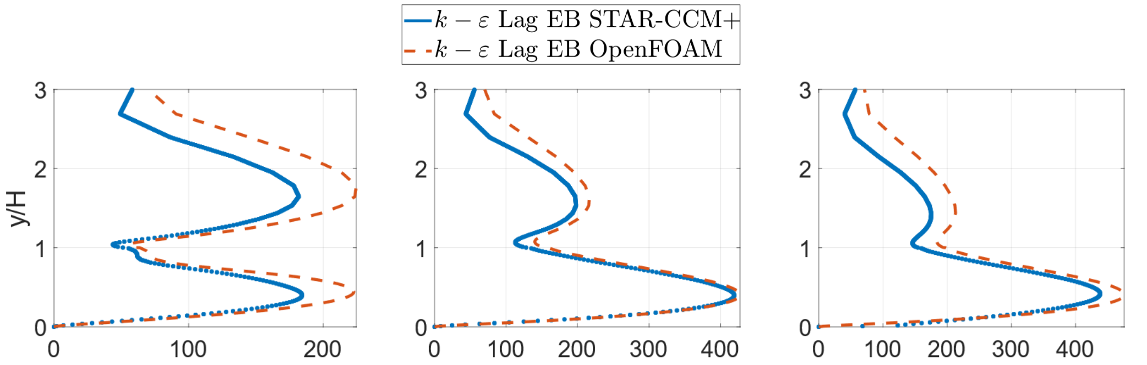

(a) (b) (c)

Figure 5. Turbulent viscosity ratio, ν_t/ν: (a) x/H = 1, (b) x/H = 4, (c) x/H = 6

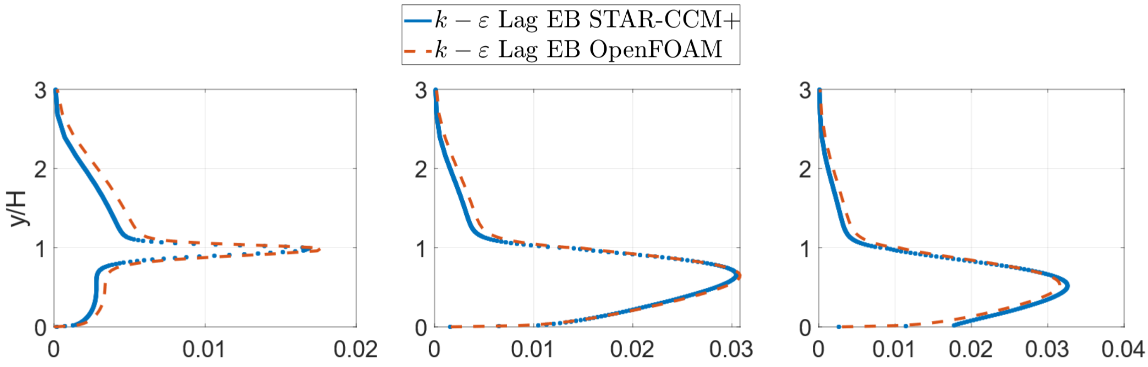

(a) (b) (c)

Figure 6. Normalized turbulent kinetic energy, k/U_{ref}^2: (a) x/H = 1, (b) x/H = 4, (c) x/H = 6

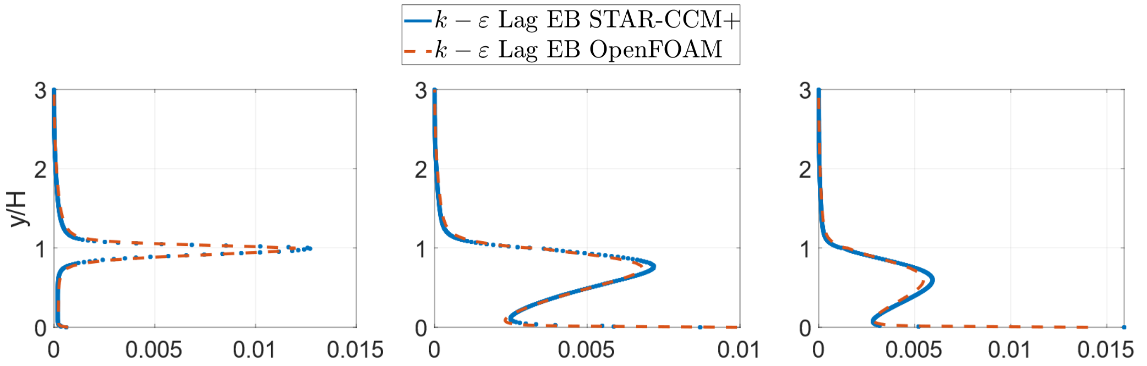

(a) (b) (c)

Figure 7. Normalized turbulent dissipation rate, $\varepsilon/(U_{\mathrm{ref}}^3/H)$: (a) x/H = 1, (b) x/H = 4, (c) x/H = 6

authors, who have no access to the source code of STAR-CCM+®. However, we would like to point out that at channel center, before and after the step, φ calculated with OpenFOAM® is close to the expected value of 2/3, which corresponds to isotropic turbulence. In contrast, the values obtained with STAR-CCM+® are generally lower, approximately around 0.4. Therefore, it is believed that the model implemented in OpenFOAM® returns more truthful values of the Lag parameter.

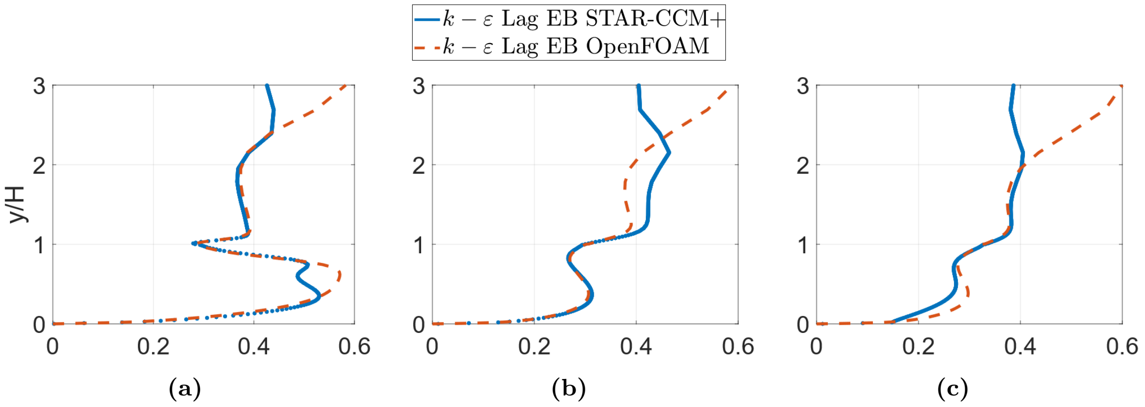

Figure 8. Lag parameter, φ: (a) x/H = 1, (b) x/H = 4, (c) x/H = 6

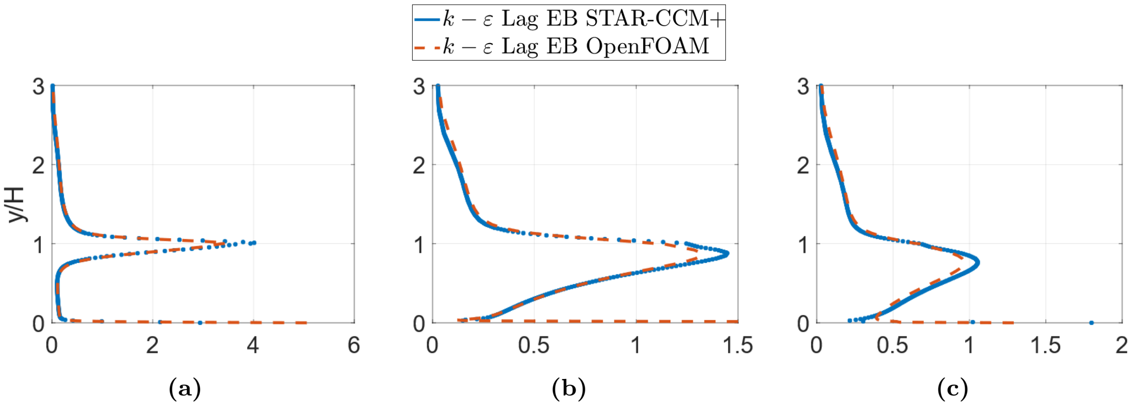

Figure 9. Normalized strain rate magnitude, $\tilde{S}/(U_{\text{ref}}/H)$: (a) x/H = 1, (b) x/H = 4, (c) x/H = 6

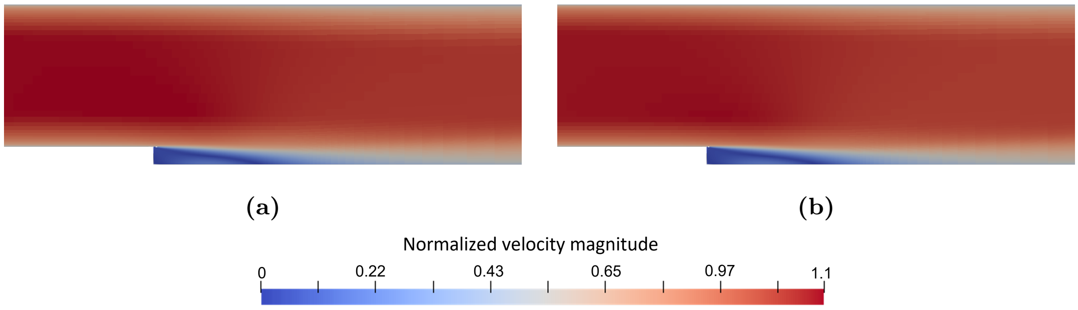

Figure 10. Contours of normalized velocity magnitude, U/U_{ref}: (a) OpenFOAM®, (b) STAR-CCM+®

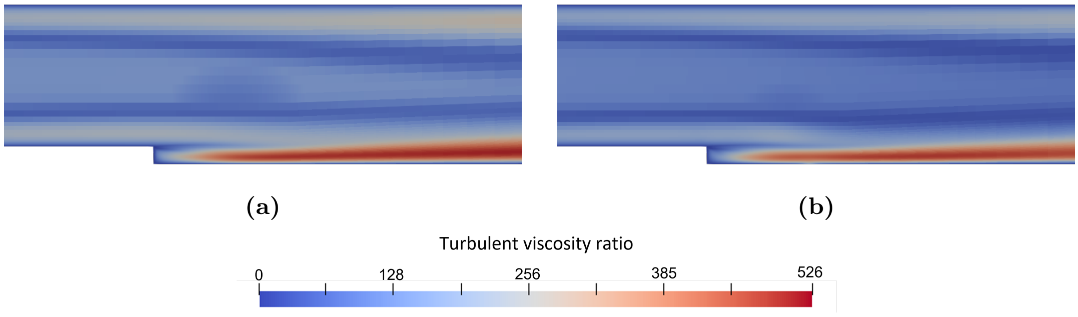

Figure 11. Contours of turbulent viscosity ratio, ν_t/ν: (a) OpenFOAM®, (b) STAR-CCM+®

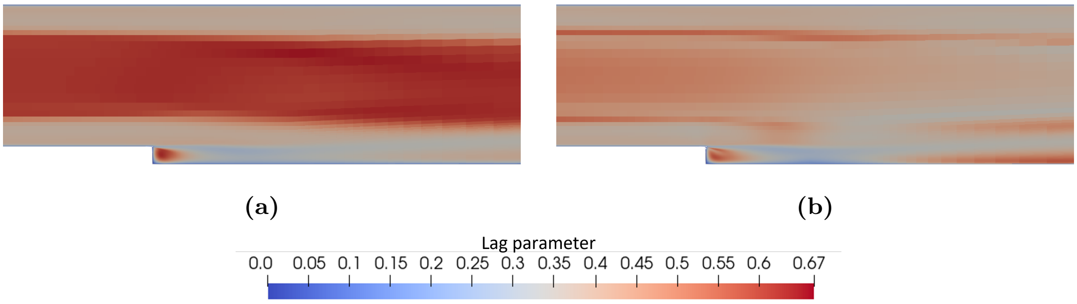

Figure 12. Contours of Lag parameter, φ. (a) OpenFOAM®, (b) STAR-CCM+®

3.2. **Benchmark case: 90° pipe bend.** In the second benchmark case, the 3D geometry of the pipe domain and mesh have been created using STAR-CCM+® and then imported into OpenFOAM®. As for the previous benchmark case, a steady-state incompressible, isothermal flow of a Newtonian fluid is simulated. The geometry is shown in Fig. 13a, while the mesh on a pipe section in Fig. 13b. The numerical settings are the same as in the BFS case. The position of the inlet guarantees fully developed flow before the bend so the position of the outlet guarantees the same on this section. The boundary conditions are the same described by Tunstall et al. [20], i.e. a Reynolds number based on the pipe's diameter $Re_D = 34000$ and no-slip at the walls. Uniform values of the quantities were imposed on the inlet section, with k evaluated by `turbulentIntensityKineticEnergyInlet` considering a turbulence intensity value $I = 10\%$, and epsilon by `turbulentMixingLengthDissipationRateInlet` with a mixing length value $\ell = 0.07D$.

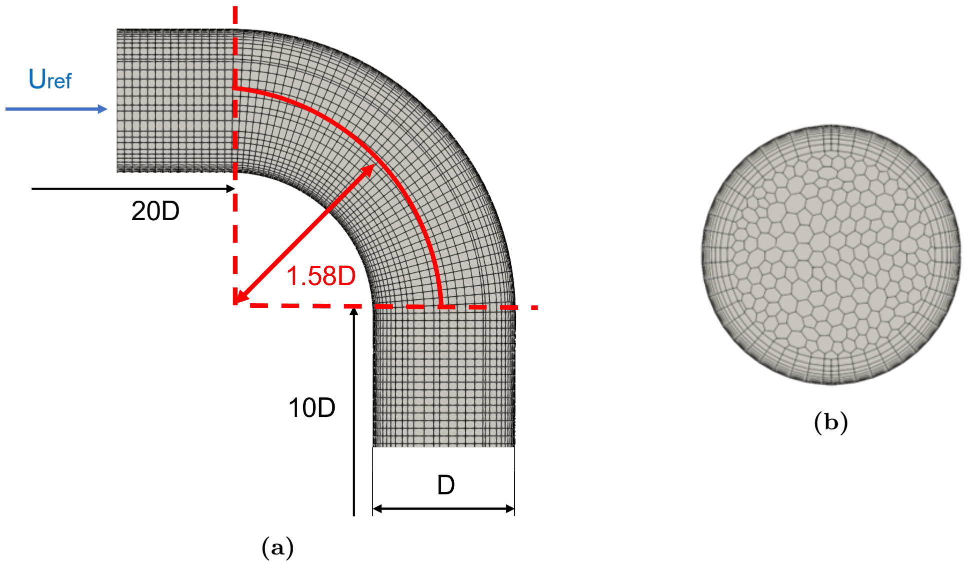

Figure 13. 90° pipe bend: (a) Geometry with relative dimensions, (b) Mesh detail

The results have been nondimensionalized with a reference velocity, U_{ref}, corresponding to the uniform pipe's inlet velocity. The qualitative comparison between the velocity results obtained with OpenFOAM® and STAR-CCM+® using the $k - \varepsilon$ Lag EB model is shown in Fig. 14a and Fig. 14b, respectively. In addition, the contours obtained with OpenFOAM® using the $k - \omega$ SST model, and those from the LES (Large Eddy Simulation) simulation by Tunstall et al. [10] are shown in Fig. 14c and Fig. 14d, respectively.

The LES contours are much closer to those obtained with the $k - \varepsilon$ Lag EB model than those obtained with the $k - \omega$ SST, in particular downstream the curve. The relative difference between the results from the two codes for the $k - \varepsilon$ Lag EB model, is shown in Fig. 15. Apart from a small region near the wall bend, the difference is below 6% everywhere. The discrepancy mentioned before may be due to the different wall treatment, i.e. wall functions, between OpenFOAM® and STAR-CCM+®.

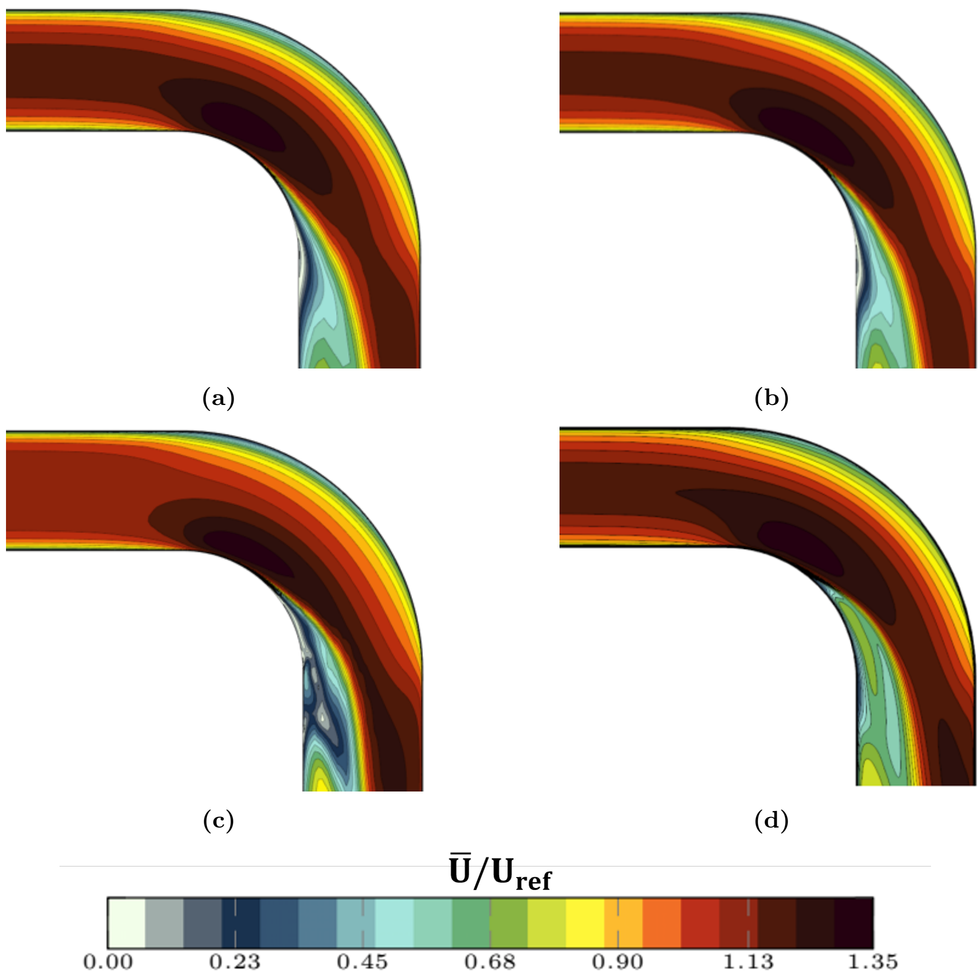
(a)

(b)

(c)

(d)

Figure 14. Normalized velocity contour: (a) Lag EB OpenFOAM®, (b) Lag EB STAR-CCM+®, (c) $k - \omega$ SST OpenFOAM® and (d) LES (reproduced from [10])

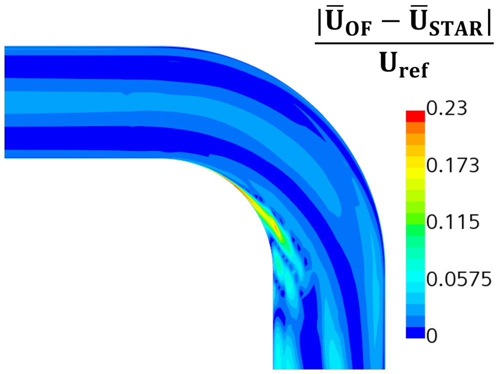

Figure 15. Relative difference between the velocity computed with OpenFOAM® and STAR-CCM+®

Finally, a quantitative comparison of the flow profile downstream the bend is presented in Fig. 16. Here, the LES results from Tunstall et al. [20] and the experimental data from Kalpakli and Orlu [21] are plotted together with the results for the $k - \varepsilon$ Lag EB model computed with both OpenFOAM® and STAR-CCM+® and those for the $k - \omega$ SST computed with OpenFOAM®. It can be seen that not only are the results of the $k - \varepsilon$ Lag EB model in almost perfect agreement between OpenFOAM® and STAR-CCM+® but that these also better agree with the experimental and LES results than the $k - \omega$ SST model, as found in [10], too.

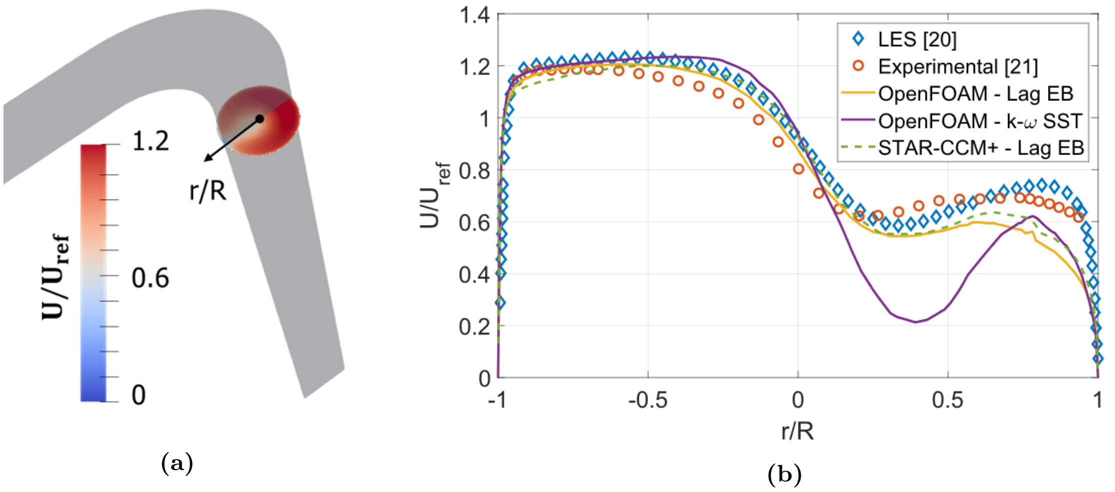

Figure 16. Normalized velocity magnitude downstream of the bend: (a) Contour with OpenFOAM® (b) Profile along the highlighted line

4. Conclusions and perspective

This paper presents the implementation of the Lag Elliptic Blending turbulence model in OpenFOAM®. Verification was conducted by comparing results from two benchmark cases (backward-facing step and 90° pipe bend) with those obtained using the commercial software STAR-CCM+®, which also features the same model. Although minor discrepancies between the two codes were observed, the verification process can be deemed satisfactory. The only unresolved issue pertains to the lag parameter, which, in the case of the backward-facing step, exhibits lower values at the channel core in STAR-CCM+® compared to the expected isotropic turbulence values. Conversely, in OpenFOAM® implementation, the lag parameter aligns with the anticipated isotropic values. A consistency check on the eddy viscosity calculation has also been performed to verify the correct implementation of ν_t.

For the 90° pipe bend case, the Lag EB model demonstrates closer agreement with experimental and LES data than the $k-\omega$ SST model, consistent with findings by Tunstall et al. [10]. Based on the obtained results, it can be concluded that the Lag EB model implementation in OpenFOAM® is accurate.

Nomenclature

Roman letters

A_{ij}	Anisotropy tensor, Eqn. 7	(−)
D	Diameter	(m)
ebf	Elliptic blending factor	(−)
H	Height	(m)
k	Turbulent kinetic energy	(m^2/s^2)
P	Turbulent kinetic energy production, Eqn. 3	(m^2/s^3)
p	Pressure	(Pa)
t	Time	(s)
T_{lim}	Limiter temporal scale, Eqn. 13	(s)
U	Average velocity	(m/s)
x	Generic coordinate	(m)
$\mathbf{n}$	Wall-normal unity vector	(−)
L	Turbulent length scale, Eqn. 11	(s)
$\tilde{S}$	Strain rate magnitude, $\tilde{S} = \sqrt{2S_{ij}S_{ij}}$	(1/s)
S_{ij}	Strain rate tensor, Eqn. 3	(1/s)
$\tilde{W}_{ij}$	Modified vorticity tensor, Eqn. 8	(1/s)
W_{ij}	Vorticity tensor	(1/s)

Greek letters

ν	Kinematic viscosity	(m^2/s)
ω	Turbulent specific dissipation rate	(1/s)
ρ	Density	(kg/m^3)
τ	Turbulent time scale	(s)
ε	Turbulent kinetic energy dissipation rate	(m^2/s^3)
φ	Lag parameter, Eqn. 6	(−)

Non-dimensional numbers

Re	Reynolds number	(−)

Abbreviations and acronyms

BFS	Backward-facing step
CFD	Computational Fluid Dynamics
EB	Elliptic Blending
EBRSM	Elliptic Blending Reynolds Stress Models
LES	Large Eddy Simulation
RANS	Reynolds Average Navier Stokes
RSM	Reynolsd Stress Models
SST	Shear Stress Transport

Appendix A. Derivation of the lag parameter and the realizability constraint

The definition of φ is given in Eqn. A-1 [8,10].

$$\varphi = -\frac{1}{C_\mu}\frac{A_{ij}S_{ij}}{S}\frac{\varepsilon}{k\tilde{S}} \tag{A-1}$$

The realizability constraint of this model is based on Durbin's original proposal [22]:

$$\left|\frac{k\tilde{S}}{\varepsilon}C_\mu\varphi\right| \leq \frac{1}{\sqrt{3}} \tag{A-2}$$

This results in the constraint for the turbulent time scale $\tau = k/\varepsilon$, as shown in Eqn. A-3.

$$\frac{k}{\varepsilon} \leq \frac{1}{C_\mu\varphi\tilde{S}\sqrt{3}} \tag{A-3}$$

To ensure the realizability constraint, the definition of the turbulent viscosity of Lardeau et al. [8], $\nu_t = C_\mu\varphi k\tau$ has been expressed in the present model [10] as in Eqn. A-4:

$$\nu_t = C_\mu\varphi k \ \min\left(\sqrt{\left(\frac{k}{\varepsilon}\right)^2 + C_t^2\frac{\nu}{\varepsilon}}, \frac{1}{C_\mu\sqrt{3}\varphi\tilde{S}}\right) \tag{A-4}$$

In the above equation, the first term inside the minimum operator considers the near wall limit of k going to zero, as proposed by Durbin [23] and also used by Billard [13].

Durbin proposed in 1991 [24] that substituting the square of the turbulent velocity scale, typically denoted as k^2 in standard turbulence models, with the square of the velocity component normal to the wall, $\overline{v'^2}$, could improve accuracy near the wall. In his formulation, $\nu_t = C_\mu\overline{v'^2}\tau$. To maintain consistency with the kinematic viscosity outlined in Eqn. 12, $\overline{v'^2} \sim \varphi k$. Consequently, for isotropic turbulence, when $\overline{u'^2} = \overline{v'^2} = \overline{w'^2} = \frac{2}{3}k$, the lag parameter φ assumes a value of $\sim \frac{2}{3}$, aligning with our simulation results.

Appendix B. Consistency check on the viscosity ratio - BFS case

A consistency check has been conducted on the turbulent viscosity ratio in the BFS case, akin to the approach outlined by Alletto in [25].

Starting from the turbulent viscosity definition in Eqn. 12 , the eddy viscosity ratio can be obtained from computed values of φ, k, ε, and $\tilde{S}$ using a MATLAB script. These values have been then compared with those extracted directly from OpenFOAM® across the three investigated sections. The comparison revealed very good agreement between the data computed with OpenFOAM® and the values obtained from the script. The consistency check has also been written in a Python script, which can be found together with the MATLAB script and data in the provided case folder of BFS.

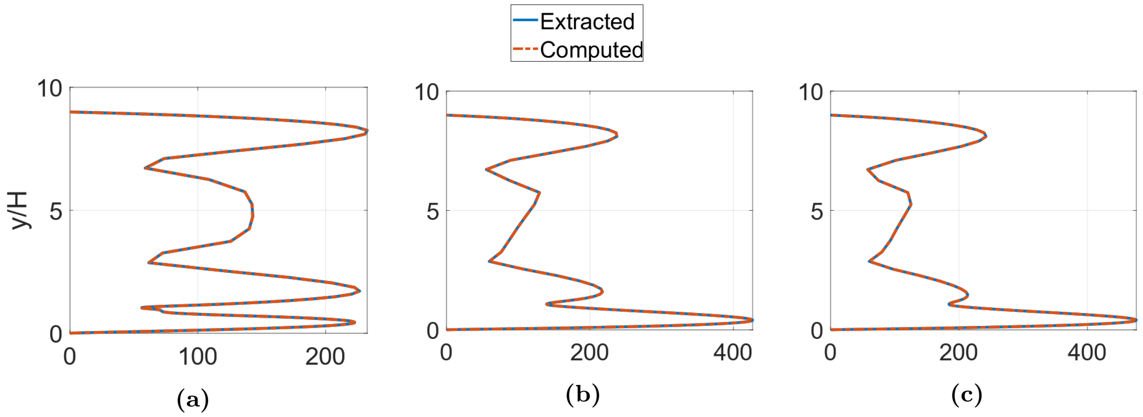

Figure 17. Turbulent viscosity ratio, ν_t/ν: (a) x/H = 1, (b) x/H = 4, (c) x/H = 6

Author contributions. Conceptualization: LM and LS; data curation: EG; formal analysis: EG; funding acquisition: LS; investigation: LM and EG; methodology: LM and EG; project administration: LS; resources: LS and GB; software: LM and EG; supervision: LM and LS; validation: LM and EG; visualization: EG; writing – original draft: EG and LM; writing – review and editing: LS, GB and AB. All authors have read and agreed to the published version of the manuscript.

References

[1] R. Difonzo, E. Gajetti, L. Savoldi, and N. Fathi, "Assessment of different RANS turbulence models in mini-channels for the cooling of MW-class gyrotron resonators," *International Journal of Heat and Mass Transfer*, vol. 193, p. 122922, 2022.

[2] W. M. H. K. Versteeg, *An Introduction to Computational Fluid Dynamics: the finite volume method.* Pearson Education Limited, 2007.

[3] P. A. Durbin, "Elliptic blending model: A new near-wall Reynolds-stress turbulence closure," *Journal of Fluid Mechanics*, vol. 249, pp. 465–498, 1993.

[4] R. Manceau and K. Hanjalić, "Elliptic blending model: A new near-wall Reynolds-stress turbulence closure," *Physics of Fluids*, vol. 14, pp. 744–754, 2002.

[5] S. Lardeau and R. Manceau, "Computations of complex flow configurations using a modified elliptic-blending Reynolds-Stress model," *10th International ERCOFTAC Symposium on Engineering Turbu lence Modelling and Measurements*, 2014.

[6] https://develop.openfoam.com/Development/openfoam/-/tree/OpenFOAM-v2206/src/TurbulenceModels/turbulenceModels/RAS/EBRSM.

[7] M. Stöllinger, R. Roy, and N. Ashton, "Application of an Elliptic Blending Reynolds Stress Model in Attached and Separated flows," *22nd AIAA Computational Fluid Dynamics ConferenceS*, 2015.

[8] S. Lardeau and F. Billard, "Development of an elliptic-blending lag model for industrial applications," *54th AIAA Aerospace Sciences Meeting*, 2016.

[9] A. Revell, S. Benhamadouche, T. Craft, and D. Laurence, "A Stress-Strain Lag Eddy Viscosity Model for Unsteady Mean Flow," *International Journal of Heat and Fluid Flow*, vol. 27, pp. 821–830, 10 2006.

[10] R. Tunstall, S. Lardeau, D. Laurence, and R. Prosser, "An elliptic blending lag model for flows in thermal-hydraulics systems," *ETMM11*, 2016.

[11] Siemens Digital Industries Software, "Simcenter STAR-CCM+, version 2022.1.1," Siemens 2022. [Online]. Available: https://www.plm.automation.siemens.com/global/en/products/simcenter/STAR-CCM.html

[12] R. Biswas, P. A. Durbin, and G. Medic, "Development of an elliptic blending lag $k-\omega$ model," *International Journal of Heat and Fluid Flow*, vol. 76, pp. 26–39, 2019.

[13] F. Billard and D. Laurence, "A robust $k-\varepsilon-v2/k$ elliptic blending turbulence model applied to near-wall, separated and buoyant flows," *International Journal of Heat and Fluid Flow*, vol. 33, pp. 45–58, 2012.

[14] D. Laurence, J. Uribe, and S. Utyuzhnikov, "A robust formulation of the v2-f model," *Flow, Turbulence and Combustion*, vol. 73, pp. 169–185, 03 2005.

[15] F. Archambeau, N. Méchitoua, and M. Sakiz, "Code_saturne: a finite volume code for the computation of turbulent incompressible flows," 2022. [Online]. Available: https://www.code-saturne.org/documentation/7.3/theory.pdf

[16] Siemens Digital Industries Software, "Simcenter STAR-CCM+ User Guide v. 2022.1.1," Siemens 2022.

[17] R. Manceau, "Recent progress in the development of the Elliptic Blending Reynolds-stress model," *International Journal of Heat and Fluid Flow*, vol. 51, pp. 195–220, 2015, theme special issue celebrating the 75th birthdays of Brian Launder and Kemo Hanjalic.

[18] https://turbmodels.larc.nasa.gov/backstep_val.html.

[19] https://develop.openfoam.com/Development/openfoam/-/tree/OpenFOAM-v2306/tutorials/incompressible/simpleFoam/backwardFacingStep2D.

[20] R. Tunstall, D. Laurence, R. Prosser, and A. Skillen, "Benchmarking LES with wall-functions and RANS for fatigue problems in thermal–hydraulics systems," *Nuclear Engineering and Design*, vol. 308, pp. 170–181, 11 2016.

[21] A. Kalpakli and R. Örlü, "Turbulent pipe flow downstream a 90° pipe bend with and without superimposed swirl," *International Journal of Heat and Fluid Flow*, vol. 41, pp. 103–111, 2013, eTMM9.

[22] P. A. Durbin, "On the k-3 stagnation point anomaly," *International Journal of Heat and Fluid Flow*, vol. 17, pp. 89–90, 1996.

[23] P. Durbin, "Nonlocal effects in single point closure," in *Proc. 3rd TRA Conf., Seoul*, 1996.

[24] P. A. Durbin, "Near-wall turbulence closure modeling without "damping functions"," *Theoretical and Computational Fluid Dynamics*, vol. 3, no. 1, pp. 1–13, Sep. 1991.

[25] M. Alletto, "Verification and Validation of the Spalart Allmaras Model with Rotation and Curvature Correction for Incompressible and Compressbile Flows," *OpenFOAM® Journal*, vol. 3, p. 159–176, Nov. 2023.